Modeling the Phase Behavior of H_2S + *n*-Alkane Binary Mixtures Using the SAFT-VR+D Approach

M. Carolina dos Ramos, Kimberly D. Goff, Honggang Zhao, and Clare McCabe*

Department of Chemical Engineering, Vanderbilt University, Nashville, Tennessee 37235

Received: January 16, 2008; Revised Manuscript Received: April 4, 2008

A statistical associating fluid theory for potential of variable range has been recently developed to model dipolar fluids (SAFT-VR+D) [Zhao and McCabe, *J. Chem. Phys.* **2006**, 125, 104504]. The SAFT-VR+D equation explicitly accounts for dipolar interactions and their effect on the thermodynamics and structure of a fluid by using the generalized mean spherical approximation (GMSA) to describe a reference fluid of dipolar square-well segments. In this work, we apply the SAFT-VR+D approach to real mixtures of dipolar fluids. In particular, we examine the high-pressure phase diagram of hydrogen sulfide + *n*-alkane binary mixtures. Hydrogen sulfide is modeled as an associating spherical molecule with four off-center sites to mimic hydrogen bonding and an embedded dipole moment (μ) to describe the polarity of H_2S. The *n*-alkane molecules are modeled as spherical segments tangentially bonded together to form chains of length *m*, as in the original SAFT-VR approach. By using simple Lorentz−Berthelot combining rules, the theoretical predictions from the SAFT-VR+D equation are found to be in excellent overall agreement with experimental data. In particular, the theory is able to accurately describe the different types of phase behavior observed for these mixtures as the molecular weight of the alkane is varied: type *III* phase behavior, according to the scheme of classification by Scott and Konynenburg, for the H_2S + methane system, type II^A (with the presence of azeotropy) for the H_2S + ethane and + propane mixtures; and type *I* phase behavior for mixtures of H_2S and longer *n*-alkanes up to *n*-decane. The theory is also able to predict in a qualitative manner the solubility of hydrogen sulfide in heavy *n*-alkanes.

I. Introduction

Sulfur compounds can be found in many natural gas and petroleum reservoirs (H_2S in particular is formed in the desulphurization process to sweeten the distillate products[1]) and are widely recognized as one of the most undesirable polluting agents in the petrochemical industry. For example, they can deactivate the catalyst in the catalytic cracking process and can cause the deposition of heavy organic molecules such as asphaltenes, which leads to corrosion in wells, pipelines, and refining equipment.[2] As a result, because of quality regulations and environmental restrictions, these compounds must be removed from the final products during the refining process.[3]

Knowledge of the thermodynamic properties and phase behavior of hydrocarbon systems containing sulfur compounds is therefore very important to the petrochemical industry and has resulted in a number of experimental studies to determine the thermodynamic properties of these mixtures. Most of this work has focused on the phase behavior of binary mixtures of hydrogen sulfide with *n*-alkanes, such as mixtures of H_2S with methane,[4,5] ethane,[6–8] propane,[9–13] *n*-butane,[14] *iso*-butane,[14] *n*-pentane,[15] *n*-hexane,[16] *n*-heptane,[17–19] *n*-decane,[20] and the solubilities of hydrogen sulfide in heavier *n*-alkanes.[20–22] Other important mixtures in the petrochemical industry involving H_2S have also been studied, such as the H_2S + water[23] and H_2S + carbon dioxide[24] systems. However, these experimental studies are limited to low temperature and pressure conditions because pure hydrogen sulfide decomposes at temperatures above 444 K,[5] thus making obtaining experimental data at high temperatures both difficult and unsafe. It would therefore be desirable to have reliable information on the thermodynamics and phase behavior of these systems from a theoretical approach.

From a modeling point of view, hydrogen sulfide is a very interesting molecule with which to study the influence of the permanent dipole moment on the thermodynamics and phase behavior. Polar interactions can greatly affect the phase behavior of pure components and their mixtures and so a nonideal phase behavior is expected for H_2S + alkane systems.[4] This is illustrated by the type *III* phase behavior[25,26] exhibited by the hydrogen sulfide + methane binary mixture, for which liquid−liquid immiscibility is observed at all temperatures and is associated with a greater disparity in intermolecular forces.[27] Nonideality is also seen as the length of the alkane chain is increased to ethane[6–8] and propane,[12] with azeotropy being observed, indicating large positive deviations from Raoult's law.[27] Additionally, a pressure maximum reappears in the gas−liquid critical line for the hydrogen sulfide + *n*-hexane and heavier alkane systems.[6] Predicting the correct phase behavior for the hydrogen sulfide + alkane binary mixtures is therefore a challenging problem because of the complexity displayed in the phase behavior of these systems.

Typically, the calculation of phase equilibrium in multicomponent systems is performed using empirical equations of state. However, the parameters involved are necessarily fitted to limited thermodynamic conditions that restrict the applicability of these equations. Over the past decade, an important advance in the prediction of the thermodynamic properties of fluids has been achieved through the application of statistical mechanics based approaches. Molecular based equations of state, such as those derived from the statistical associating fluid theory (SAFT), provide a framework in which the different microscopic effects such as nonsphericity and association interactions can

* Corresponding author. Email: c.mccabe@vanderbilt.edu.

10.1021/jp800397n CCC: $40.75
Published on Web 07/16/2008

be estimated and quantified separately, leading to a predictive and reliable equation of state applicable to complex systems. The SAFT equation was originally proposed by Chapman et al.[28,29] on the basis of Wertheim's thermodynamic perturbation theory[30–33] and is written as a sum of different contributions to the Helmholtz free energy. Since its development, the SAFT equation has been applied to describe a wide range of fluids, and many variations of the original expressions have been introduced.[34–36]

The SAFT approach has been applied to study multipolar fluids, such as water,[37–40] refrigerants,[41] carbon dioxide, and its mixtures,[40,42–46] in which the dipolar and quadrupolar interactions are usually treated in an effective manner via the segment size and energy parameters and/or through association interaction parameters. However, the SAFT approach has been extended in several studies to incorporate the dipolar interaction by adding a dipolar contribution term to the expression for the Helmholtz free energy.[47–53] In these extensions, the dipolar contribution is typically described using the μ expansion proposed by Gubbins and Gray[54] or the Padé approximation of Stell et al.,[55] in which the nonspherical dipolar molecules are approximated by spherical molecules and the orientation of the dipolar interaction is not taken into account. Alternatively, expressions for incorporating dipolar interactions can be derived from molecular simulation as in the work of Gross and Vrabec[51] who proposed a dipolar term based on simulation data for the vapor−liquid equilibria of the two-center Lennard-Jones plus point dipole fluid. In order to model polar chain fluids, Jog et al.[56,57] developed a SAFT EOS that includes the dipole moment in alternate chain monomers and was later applied by Tumakaka and Sadowski[58] to the perturbed chain SAFT (PC-SAFT) equation in order to describe mixtures of polar and nonpolar fluids. More recently, Karakatsani et al.[52,53] proposed a polar PC-SAFT approach based on the perturbation theory of Stell and co-workers that uniformly distributes the dipole over all segments, rather than being located in certain segments of the molecule as in the work of Jog et al. Although in these approaches the molecules are not treated as spherical, the dipolar interactions are still included by adding a contribution to the free energy, and therefore, the effect of the dipole on the structure and in turn the thermodynamic properties is not explicitly considered.

More recently, we have proposed the SAFT-VR+D equation of state[59,60] in which the dipolar interactions and their effect on the structure of the fluid are taken into account by using a dipolar square-well fluid as the monomer fluid within the framework of the SAFT approach. Hence, the potential of the reference state is composed of two parts: a square-well (SW) isotropic potential and an anisotropic dipolar potential. The SAFT-VR+D approach has been validated through extensive comparison with computer simulation data for model monomer and chain dipolar fluids and found to provide a good representation of the phase behavior.[59,60] Additionally, we have also applied the SAFT-VR+D approach to model associating dipolar fluids and water.[60] By modeling water as a dipolar associating fluid, we can explicitly (as opposed to treating the solvent as a dielectric continuum) represent the solvent in electrolyte systems.[61]

In this work, we have applied the SAFT-VR+D approach to describe mixtures of polar + nonpolar systems based on the work of Adelman and Deutch[62] and studied the thermodynamic properties and phase behavior of the H_2S + *n*-alkane binary mixtures. H_2S is very similar to water in that both molecules possess polar and association interactions, which need to be incorporated into the molecular model; Benavides and Guevara reached similar conclusions in their study of water and ammonia with a dipolar square-well model.[63] We have obtained the molecular parameters for pure polar hydrogen sulfide using the SAFT-VR+D equation and those for the *n*-alkanes are taken from earlier work.[64,65] The unlike interaction parameters between different compounds are obtained using simple Lorentz−Berthelot combining rules, and so, only the pure component intermolecular parameters are fitted to experimental data. In this manner, the ability of the theoretical approach to predict the rich phase behavior displayed by the H_2S + *n*-alkane systems can be tested. In addition, the effect of pressure and molecular weight of the *n*-alkane on the solubility of H_2S is studied.

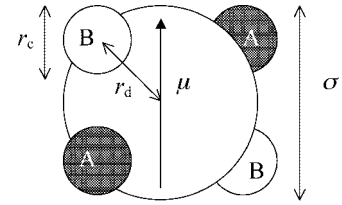

Figure 1. Schematic representation of the model used to describe the hydrogen sulfide molecule: a spherical segment with a dipole moment μ embedded in the centre of the monomer and four square-well bonding sites (two of type A and two of type B) placed at a distance r_d off-centre of a sphere of hard-core diameter σ. Only the A−B bonding interaction is allowed when the two sites are closer than a distance r_c apart.

The rest of the paper is organized as follows: the molecular model and theory are described in section II; the results and discussion are presented in section III; and conclusions are given in section IV.

II. Molecular Model and Theory

The potential models used to describe hydrogen sulfide in the literature can be divided into two main groups: three-site[66] and four-site models.[67,68] Jorgensen[66] first proposed the three-site potential model, similar to the TIP3P model for water,[69] which considers hydrogen sulfide as a Lennard-Jones sphere with two positive point charges on the hydrogen atoms and one negative point charge on the sulfur atom. The four site model was proposed by Forester et al.[67] and has an additional partial charge, located on the bisector H−S−H angle, which is similar to the TIP4P-like geometry proposed for water.[69] Both the three-site and the four-site models have been used to model hydrogen sulfide in molecular simulations,[70–74] as well as in other versions of SAFT that do not explicitly include the dipole moment.[75–77] In this work, we consider the four-site potential model as it most physically mimics the H_2S molecule. Within the SAFT-VR+D approach, H_2S is therefore described as an associating dipolar square-well segment of diameter σ_{11}, that interacts via an embedded dipole moment μ_{11}, a square-well dispersion potential of a depth ε_{11} and range λ_{11}, and four off-center short-range attractive sites to describe the self-association. Two sites of type A represent the hydrogen atoms, and two sites of type B represent the lone pairs of electrons on the sulfur atom. Only A−B site−site interactions are allowed. The sites are placed at a distance $r_d = 0.25$ from the center of the sphere and have a cutoff range of r_c so that an attractive energy ε^{HB} is realized if sites are closer than a distance r_c apart. This model is schematically represented in Figure 1.

The *n*-alkane family members, which are nonassociating and nonpolar molecules, are described by four molecular parameters: the number of segments forming the model chain molecule m_2, the segment size σ_{22}, and the depth ε_{22} and range λ_{22} of the square-well dispersion interaction.

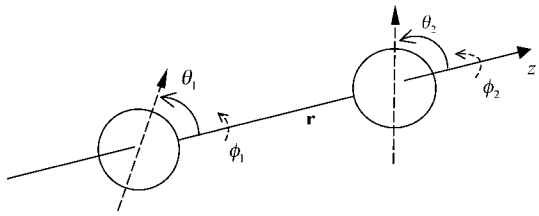

Figure 2. Schematic representation of the interdipole site coordinate system, with polar axis along *r*.[80]

In the SAFT-VR+D approach, the inclusion of the dipole−dipole interactions are accounted for through the dipole moment μ and the orientation of the dipoles which is determined by the azimuthal θ and polar ϕ angles of the intersegment axis along *r*, as shown in Figure 2.[80] Therefore, the pair potential for the dipolar associating fluids studied is defined as

$$u_{ij}(\mathbf{r}_{ij}\mathbf{w}_1\mathbf{w}_2) = u_{ij}^{HS}(r_{ij};\sigma_{ij}) - \varepsilon_{ij}\varphi_{ij}^{SW}(r_{ij};\lambda_{ij}) + u_{ij}^{\text{dipole}}(\mathbf{r}_{ij}\mathbf{w}_1\mathbf{w}_2) + \sum_{A_i}\sum_{B_j} u_{A_iB_j}^{HB}(\mathbf{r}_{ij}\Omega_1\Omega_2) \quad (1)$$

where $\mathbf{r}_{ij}$ is the vector between the center of monomers *i* and *j*; $r_{ij} = |\mathbf{r}_{ij}|$ is the distance between segments of species *i* and *j*; $\mathbf{w}_i = (\theta_i,\varphi_i)$ is the set of angles that defines the orientation of the dipole moment in the monomer of species *i*; and Ω_i is the orientation of the association site *i* relative to the vector $\mathbf{r}_{ij}$. As in the SAFT-VR equation for mixtures,[64,81] the monomer−monomer isotropic potential consists of a hard sphere repulsive interaction $u_{ij}^{HS}(r_{ij};\sigma_{ij})$ defined by,

$$u_{ij}^{HS}(r_{ij};\sigma_{ij}) = \begin{cases} \infty & \text{if} \quad r_{ij} < \sigma_{ij} \\ 0 & \text{if} \quad r_{ij} > \sigma_{ij} \end{cases} \quad (2)$$

and an attractive term $-\varepsilon_{ij}\varphi_{ij}^{SW}(r_{ij};\lambda\text{ij})$ modeled by a square-well potential of depth ε_{ij} and shape $\varphi_{ij}^{SW}(r_{ij};\lambda_{ij})$ defined by

$$\varphi_{ij}^{SW}(r_{ij};\lambda_{ij}) = \begin{cases} 1 & \text{if} \quad \sigma_{ij} < r_{ij} < \lambda_{ij}\sigma_{ij} \\ 0 & \text{if} \quad r_{ij} > \lambda_{ij}\sigma_{ij} \end{cases} \quad (3)$$

where λ_{ij} is the parameter associated with the range of the square-well potential. The dipole−dipole potential $u_{ij}^{\text{dipole}}(\mathbf{r}_{ij}\mathbf{w}1\mathbf{w}2)$ is a long-range anisotropic interaction, which can be expressed as

$$u_{ij}^{\text{dipole}}(\mathbf{r}_{ij}\mathbf{w}_1\mathbf{w}_2) = -\frac{\mu_i\mu_j}{r_{ij}^3} D_{ij}(\mathbf{n}_1\mathbf{n}_2\hat{\mathbf{f}}_{ij}) \quad (4)$$

The association potential $u_{A_iB_j}^{HB}$ models site−site association interactions between molecules through an anisotropic short-range square-well interaction, where A_i and B_j are interacting associating sites on species *i* and *j*, respectively.

Within the SAFT framework, the Helmholtz free energy *A* can be written in the form

$$\frac{A}{Nk_BT} = \frac{A^{\text{IDEAL}}}{Nk_BT} + \frac{A^{\text{MONO}}}{Nk_BT} + \frac{A^{\text{CHAIN}}}{Nk_BT} + \frac{A^{\text{ASSOC}}}{Nk_BT} \quad (5)$$

where *N* is the total number of molecules, *T* is the temperature, k_B is the Boltzmann constant, A^{IDEAL} is the free energy of the ideal fluid, A^{MONO} is the contribution due to the dipolar square-well monomer fluid, A^{CHAIN} represents the free energy due to chain formation from the monomer segments, and A^{ASSOC} is the free energy contribution due to intermolecular association. We will briefly outline each contribution in turn, focusing on the dipolar contribution.

Ideal Contribution. The free energy of an ideal mixture is given by[82]

$$\frac{A^{\text{IDEAL}}}{Nk_BT} = \sum_{i=1}^{n} x_i \ln(\rho_i\Lambda_i^3) - 1 \quad (6)$$

where $\rho_i = N_i/V$ is the number density, *N* is the number of molecules, x_i is the molar fraction, and Λ_i is the thermal de Broglie wavelength of species *i*.

Monomer Contribution. The contribution to the Helmholtz free energy due to the monomer segments is given by

$$\frac{A^{\text{MONO}}}{Nk_BT} = \left(\sum_{i=1}^{n} x_i m_i\right)\frac{A^M}{N_s k_BT} = \left(\sum_{i=1}^{n} x_i m_i\right) a^M \quad (7)$$

where N_s is the total number of spherical monomers. Within the GMSA, the excess Helmholtz free energy per monomer a^M is given by the free energy per monomer of the dipolar square-well reference fluid a^{DSW} which in turn can be written as

$$a^M = a^{\text{DSW}} = a^{\text{dipole}} + a^{\text{isotropic}} \quad (8)$$

where a^{dipole} describes the contribution to the free energy due to the anisotropic dipolar interactions and $a^{\text{isotropic}}$ is written in terms of the inverse of the temperature $\beta = 1/k_BT$ within the second-order high temperature perturbation expansion of Barker and Henderson[83−85] as in the original SAFT-VR approach,[64]

$$a^{\text{isotropic}} = a^{HS} + \beta a_1 + \beta^2 a_2 \quad (9)$$

where a^{HS} is the free energy due to repulsive interactions between the hard cores, and a_1 and a_2 are the first and second order perturbation terms associated with the isotropic attractive interactions, respectively. The residual free energy of the hard-sphere mixture is obtained from the expression of Boublik[86] and Mansoori et al.[87] The mean-attractive energy associated with the first-order perturbation term is treated in the context of the M1Xb mixing rules[81] and the second-order perturbation term is obtained using the local compressibility approximation as in the original SAFT-VR approach.

In previous work,[59,60] we obtained the anisotropic dipolar contribution of an associating polar fluid from Wertheim's solution[88] of the Ornstein−Zernike equation for dipolar hard spheres and chains with mixed dipole moments using the MSA and LEXP closures. Here, we apply the SAFT-VR+D approach to study mixtures of dipolar associating fluids and nondipolar fluids, on the basis of the work of Adelman and Deutch,[62] who provided an exact solution to the MSA for simple polar mixtures. They have shown that an *n*-component polar fluid characterized by densities ρ_1, ρ_2,..., ρ_n and permanent dipole moments μ_1, μ_2,..., μ_n can be reduced to an effective one-component fluid, with an effective dipole moment $\hat{\mu}$ and an effective density $\hat{\rho}$, as follows:

$$\hat{\mu}^2 = \frac{1}{n}\sum_{i=1}^{n} \mu_i^2 \quad (10)$$

$$\hat{\rho} = \frac{1}{\hat{\mu}^2}\sum_{i=1}^{n} \mu_i^2\rho_i \quad (11)$$

In this case, the expressions for the excess thermodynamic properties of a multicomponent system within the MSA are the same as those for the pure fluid but evaluated at the effective density and effective dipole moment. In the particular limiting case where the mixture is composed of polar and nonpolar fluids, Adelman and Deutch[62] found that the dipolar terms of the correlation functions for the polar species do not depend on

the presence of nonpolar species and vice versa. In this context, the anisotropic dipolar contribution for a polar mixture is obtained using the equations for a pure fluid with an effective dipole moment and density. The reader is directed to refs 59, 60, 88 for additional details.

Therefore, the excess free energy due to the dipolar interactions is given by

$$a^{\mathrm{DIPOLE}} = -\frac{8}{\eta}\xi^2\left[\frac{(1+\xi)^2}{(1-2\xi)^4} + \frac{(2-\xi)^2}{8(1+\xi)^4}\right] \tag{12}$$

where $\xi = \kappa\eta$ and κ is the scaling parameter. κ is determined by y, the so-called strength of the dipolar effect[88]

$$3y = q_{PY}(2\kappa\eta) - q_{PY}(-\kappa\eta) \tag{13}$$

and is a dimensionless function of the temperature β, the effective density $\hat{\rho}$, and dipole moment $\hat{\mu}$

$$y = \frac{4\pi}{9}\beta\hat{\rho}\hat{\mu}^2 \tag{14}$$

q_{PY} is the dimensionless inverse compressibility of Percus−Yevick (PY), given by[88]

$$q_{PY}(\eta) = \frac{(1+2\eta)^2}{(1-\eta)^4} \tag{15}$$

where η is the packing fraction of the mixture giving by

$$\eta = \frac{\pi}{6}\hat{\rho}\left[\sum_{i=1}^{n} m_i x_i \sigma_{ii}^3\right] \tag{16}$$

Chain Contribution. The contribution to the free energy due to chain formation from the dipolar square-well monomer segments is given by

$$\frac{A^{\mathrm{CHAIN}}}{Nk_{\mathrm{B}}T} = -\sum_{i=1}^{n}(m_i - 1)\ln y_{ii}^{DSW} \tag{17}$$

where m_i is the number of segments of component i, y_{ii}^{DSW} is the dipolar square-well monomer background correlation function evaluated at hard-core contact for species i,

$$y_{ii}^{DSW}(\mathbf{r}_{ii}\mathbf{w}_1^i\mathbf{w}_2^i) = \exp[\beta u_{ii}^{DSW}(\mathbf{r}_{ii}\mathbf{w}_1^i\mathbf{w}_2^i)]g_{ii}^{DSW}(\mathbf{r}_{ii}\mathbf{w}_1^i\mathbf{w}_2^i;\rho,T) \tag{18}$$

and $g_{ii}^{DSW}(\mathbf{r}_{ii}\mathbf{w}_1^i\mathbf{w}_2^i;\rho,T)$ is the pair distribution function for the dipolar square-well molecules and is obtained from the GMSA.

In our particular case for the H_2S (1) + n-alkane (2) binary mixtures, the chain contribution is only required for the second component. In this case, the pair correlation functions of the nonpolar species are unaffected by the dipolar interactions in the polar fluid. The expressions of the chain contribution are then written in a simpler form as:

$$\frac{A^{\mathrm{CHAIN}}}{Nk_{\mathrm{B}}T} = -(m_2 - 1)\ln y_{22}^{SW}(\sigma_{22}) \tag{19}$$

where the background correlation function ($y_{22}^{SW}(\sigma_{22}) = \exp[\beta u_{22}^{SW}]g_{22}^{SW}(\sigma_{22})$) is now given for the nonpolar square-well fluid as in the original SAFT-VR approach.[64,81]

Association Contribution. The contribution to the free energy due to the association of s_i sites on a molecule of species i can be obtained from Wertheim's theory as:

$$\begin{aligned}\frac{A^{\mathrm{ASSOC}}}{Nk_{\mathrm{B}}T} &= \sum_{i=1}^{n} x_i\left[\sum_{a=1}^{s_i}(\ln X_{a,i} - \frac{X_{a,i}}{2}) + \frac{s_i}{2}\right] \\ &= x_1\left[4\left(\ln X - \frac{X}{2}\right) + 2\right]\end{aligned} \tag{20}$$

where the first sum is over species i and the second sum is over all s_i sites of type a on a molecule i. Since the only type of association considered is between the sites $A-B$ of the hydrogen sulfide molecule and no hydrogen sulfide-alkane cross association is considered, the association contribution expression can be simplified in terms of the fraction of hydrogen sulfide molecules not bonded, X. In this case, the fraction $X_{a,i}$ of molecules i not bonded at site a is given by the mass action equation as[28,29]

$$X_{a,i} = \frac{1}{1 + \rho\sum_{j=1}^{n} x_j \sum_{b=1}^{s_j} X_{b,j}\Delta_{a,b,i,j}} = X = \frac{1}{1 + 2\rho x_1 \Delta_{11}} \tag{21}$$

Here, $\Delta_{a,b,i,j}$ characterizes the association between site a on molecule i and site b on molecule j and can be written as

$$\Delta_{a,b,i,j} = K_{a,b,i,j} f_{a,b,i,j} g_{ij}^{SW}(\sigma_{ij}) = \Delta_{11} = K_{11} f_{11} g_{11}^{SW}(\sigma_{11}) \tag{22}$$

where $g_{ij}^{SW}(\sigma_{ij})$ is the contact value of the radial distribution function, $f_{a,b,i,j} = \exp(-\varphi_{a,b,i,j}/k_{\mathrm{B}}T) - 1$ is the Mayer f function for the $a-b$ site−site interaction $\varphi_{a,b,i,j}$, and $K_{a,b,i,j}$ is the volume available for bonding. The expression for the Mayer f function can be further simplified since the binary systems under examination only consider association between the molecules of component 1 (hydrogen sulfide) and is given by $f_{11} = \exp(\varepsilon_{11}^{HB}/k_{\mathrm{B}}T) - 1$. The expression for the available bonding volume is given by[28,29,79]

$$\begin{aligned}K_{11} = \; & 4\pi\left[\ln\left(\frac{r_{c_1} + 2r_{d_1}}{\sigma_{11}}\right)\left(6r_{c_1}^3 + 18r_{c_1}^2 r_{d_1} - 24r_{d_1}^3\right) + \ldots\right. \\ & \left.\left(r_{c_1} + 2r_{d_1} - \sigma_{11}\right)\left(22r_{d_1}^2 - 5r_{c_1}r_{d_1} - 7r_{d_1}\sigma_{11} - 8r_{c_1}^2 + r_{c_1}\sigma_{11} + \sigma_{11}^2\right)\right]\end{aligned} \tag{23}$$

With the expression for the Helmholtz free energy defined, thermodynamic properties, such as the chemical potential, compressibility factor, and other thermodynamic derivatives, can be easily obtained using standard thermodynamic relations. The study of phase equilibrium in mixtures also requires the determination of a number of cross interaction parameters, which account for the interactions between unlike components in the mixture. The Lorentz arithmetic mean is used for the unlike hard-core diameter,

$$\sigma_{12} = \frac{\sigma_{11} + \sigma_{22}}{2} \tag{24}$$

the unlike square-well dispersive energy is given by the Berthelot rule as follows,

$$\varepsilon_{12} = \sqrt{\varepsilon_{11}\varepsilon_{22}} \tag{25}$$

and the unlike square-well potential range is given by

$$\lambda_{12} = \frac{\lambda_{11}\sigma_{11} + \lambda_{22}\sigma_{22}}{\sigma_{11} + \sigma_{22}} \tag{26}$$

The results obtained for the mixtures of the hydrogen sulfide + n-alkanes are therefore pure predictions from the SAFT-VR+D equation, since the cross or unlike interaction parameters

TABLE 1: Optimized and Rescaled (Indicated by Subscript c) Intermolecular Parameters for Hydrogen Sulfide

m	λ	σ (Å)	ε/k_B (K)	ε^{HB}/k_B (K)	K^{HB} (Å^3)	σ_c (Å)	ε_c/k_B (K)	$\varepsilon^{HB}{}_c/k_B$(K)	$K_c{}^{HB}$ (Å^3)
1	1.6255	3.67295	212.4090	501.69791	1.5000	3.88160	204.8186	482.8249	1.760990

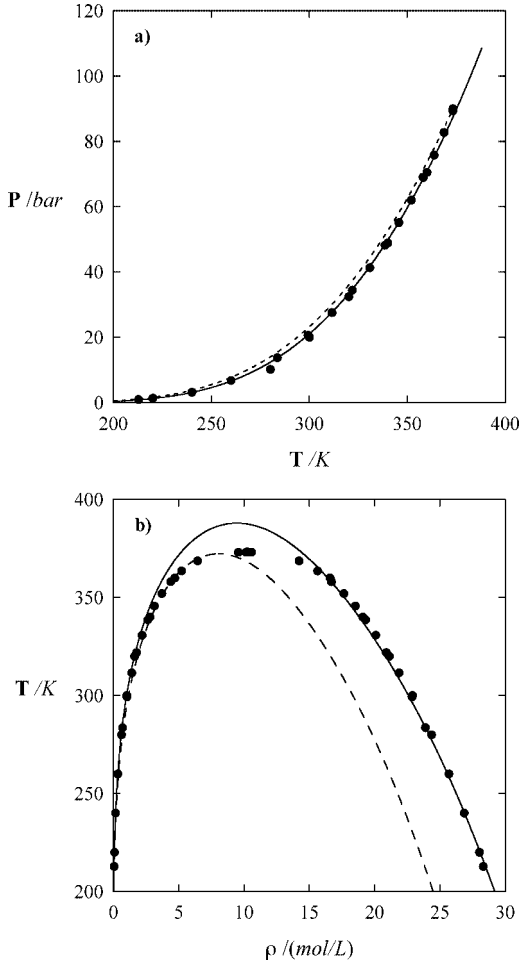

Figure 3. Vapor pressures (a) and vapor−liquid coexistence densities (b) of pure hydrogen sulfide. Circles correspond to the experimental data.[89,98,99] Solid lines and dashed lines represent the SAFT-VR+D predictions obtained with the optimized and rescaled parameters, respectively (see Table 1).

are obtained from the pure substance parameters and no experimental data for the mixtures are used to calculate the thermodynamic properties.

III. Results and Discussion

In order to study the H_2S + *n*-alkane systems, the intermolecular parameters for the pure substances first need to be defined. The hydrogen sulfide molecule is treated as a spherical segment with a fixed chain length of $m_1 = 1$ and an embedded dipole moment μ_{11}. The experimental value of the dipole moment of hydrogen sulfide, $\mu_{11} = 0.97$ Debye,[89] is used in the calculations, and the remaining intermolecular parameters are determined by fitting the theoretical predictions to experimental vapor pressure and saturated liquid density data using an annealing technique.[90,91] The optimized values for the hard-core diameter (σ_{11}), square-well potential depth (ϵ_{11}), and range (λ_{11}) parameters, as well as the association parameters ($\epsilon_{11}{}^{HB}$ and $K_{11}{}^{HB}$) are presented in Table 1. The results obtained from the SAFT-VR+D approach with this set of parameters provide a good description of the vapor pressures and coexisting densities of H_2S over a wide range of temperatures, as shown

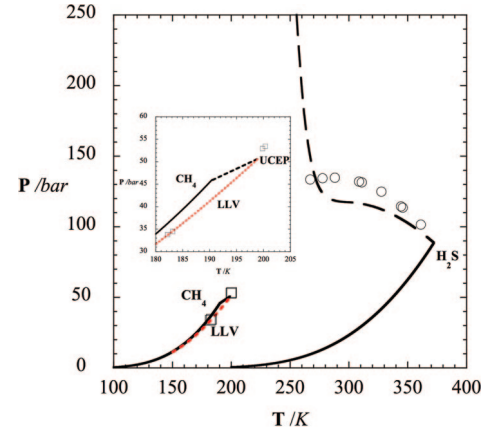

Figure 4. *PT* projection of the *PTx* surface for the H_2S (1) + methane (2) binary mixture. Circles and squares correspond to the experimental data[4,5] for the critical lines and the three-phase liquid−liquid−vapor line (LLV), respectively. Solid lines represent the SAFT-VR+D predictions for the pure component vapor pressures, long dashed lines represent the critical lines and the dashed lines correspond to the three-phase line. The inset shows the region of liquid−liquid immiscibility close to the critical point of pure methane.

in Figure 3a,b, respectively. The percentage of absolute average deviation (%AAD) for the vapor pressure was found to be 3.98%, and 5.66% for the saturated liquid density, using the whole set of experimental data. As with most engineering equations of state, the SAFT-VR+D approach does not include the long-range density fluctuations that occur near the critical point of real fluids and so, being analytical in the free energy, over predicts the critical point.[40,44,92,93] Since our interest is in the phase diagrams and critical lines of the H_2S + *n*-alkane binary mixtures, we have rescaled the intermolecular parameters to the experimental critical point of hydrogen sulfide ($T_c{}^{exp}$ = 373.3 K and $P_c{}^{exp}$ = 89.70 bar).[94] These parameters are also reported in Table 1. For the *n*-alkane family members, the set of intermolecular parameters (m_2, σ_{22}, ε_{22}, and λ_{22}) proposed previously[64,65] and which have been shown to provide an excellent description of the thermodynamic properties of this chemical family[95–97] are used.

A. Hydrogen Sulfide + Methane Binary Mixture. The *PT* projection of the *PTx* surface for the H_2S (1) + methane (2) binary mixture is shown in Figure 4. As can be seen from the figure, the phase behavior of this system is dominated by large regions of liquid−liquid (LL) immiscibility characteristic of type *III* phase behavior according to the classification scheme of Scott and van Konynenburg (SK).[25,26] This behavior is associated with a large disparity in the intermolecular forces between the components of the mixture, such as the presence of polar and association interactions between the hydrogen sulfide molecules[27] compared with the nonpolar *n*-alkanes. This system exhibits two gas−liquid (GL) critical lines; at high temperatures and pressures, a critical line starts from the critical point of the less volatile component (hydrogen sulfide at 373.3 K and 89.70 bar) and continues to lower temperatures as the pressure is increased, passing through a temperature minimum around 243 K and then extending to higher temperatures and pressures with a positive slope. This is a distinct feature characteristic of gas−gas immiscibility of the second kind.[27] At low temperatures and pressures, a second gas−liquid critical line runs from the

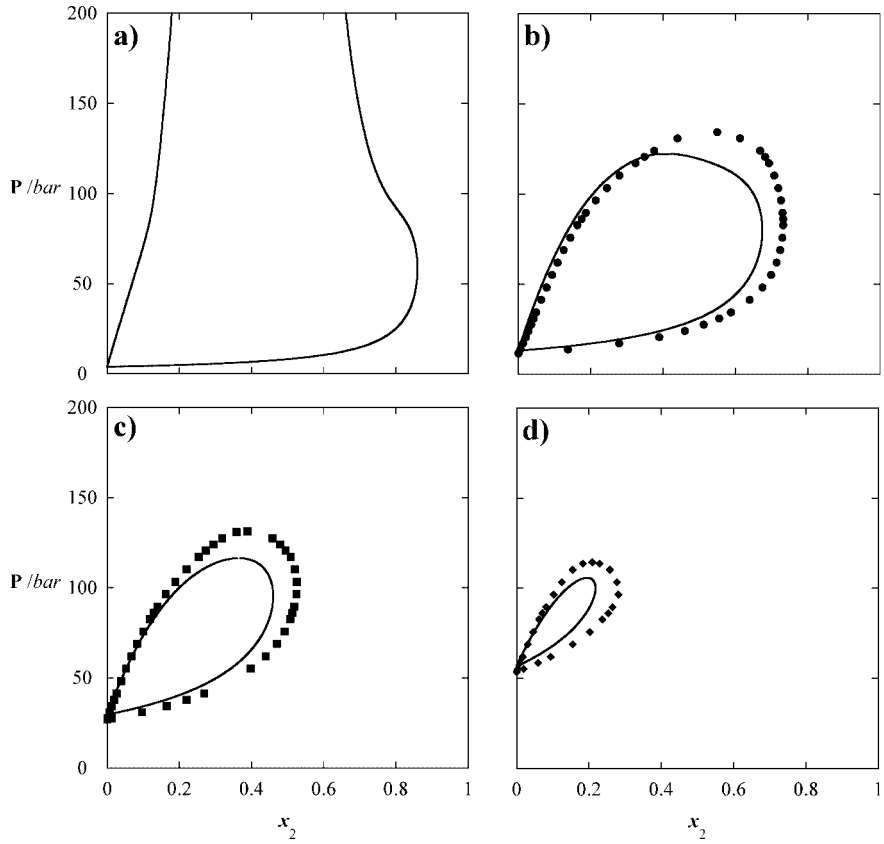

Figure 5. *Px* constant-temperature slices of the H_2S (1) + methane (2) binary mixture at 240.0 K (a), 277.59 K (b), 310.93 K (c), and 344.26 K (d). Circles correspond to the experimental data.[4,5] Solid lines represent the theoretical predictions using the SAFT-VR+D approach.

critical point of the more volatile component (methane at 190.6 K and 46.1 bar) to the upper critical end point (UCEP), close to the critical point of pure methane, where the methane-rich liquid phase becomes identical with the gas phase. From this UCEP and continuing to very-low temperatures and pressures, a three-phase line is found, where the two immiscible liquid phases coexist with a gaseous phase. This line can be seen more clearly from the inset of Figure 4a. Note that the experimental three-phase line terminates at low-temperatures at the quadruple point of 182.2 K and 33.78[4] bar, where the four phases (liquid−liquid−gas−solid) are in equilibrium. The theory is able to provide a good description of the *PT* fluid phase diagram for this mixture, although the gas−liquid critical line at high temperatures and pressures is underestimated; however, it is important to mention that we have not adjusted any of the model parameters to experimental data for the H_2S + methane mixture, and therefore, all of the theoretical results are pure predictions.

In Figure 5, we examine the constant-temperature *Px* projections of the hydrogen sulfide + methane binary mixture. The low temperature slice at 240 K is just below the minimum (243 K) in the gas−liquid critical line but still above the UCEP for this mixture. At this temperature, the system exhibits a continuous transition in the coexistence envelopes, from a gas−liquid character at low pressure to a liquid−liquid character at high pressure. This peculiar shape of the phase envelope is characteristic of liquid−liquid immiscibility as seen in type *III* phase behavior. At higher temperatures, between the minimum temperature of the gas−liquid critical line and the critical point of pure hydrogen sulfide, the system exhibits gas−liquid coexistence that extends from the vapor pressure of pure H_2S to the gas−liquid critical point of the mixture at the corresponding temperature. It is important to mention that at these temperatures, the system will exhibit a second two-phase fluid−fluid region at very high pressures, as can be inferred from Figure 5b. This feature is related to gas−gas immiscibility of the second kind. As can be seen, the SAFT-VR+D equation is able to correctly predict the type *III* phase behavior and accurately capture the transitions observed in the phase behavior of H_2S + methane as the thermodynamic conditions are varied. This system was recently studied by Aparicio-Martinez and Hall,[75] using the PC-SAFT equation with a modified Berthelot value of $k_{12} = 0.0401$ and shown to display type *I* phase behavior, indicating that the PC-SAFT equation was not able to predict the liquid−liquid immiscibility seen in this system.[27] Aparicio-Martinez and Hall also studied other H_2S + *n*-alkanes systems (ethane, propane, *n*-butane, and *n*-pentane), using system-dependent binary interaction parameters for each mixture studied, as the complex behavior of this homologous series did not allow the use of transferable parameters.

B. Hydrogen Sulfide + Ethane and Hydrogen Sulfide + Propane Binary Mixtures. In this section, we examine the phase behavior of the binary mixtures of hydrogen sulfide + ethane and hydrogen sulfide + propane. As the volatility of the hydrocarbon approaches that of the hydrogen sulfide, the nature of the critical lines is greatly affected. Additionally, these systems are known to exhibit azeotropic behavior because of the fact that ethane and propane have similar volatilities and boiling points compared with hydrogen sulfide.[27]

In Figure 6a, the *PT* projection of the *PTx* surface for the H_2S (1) + ethane (2) binary mixture is shown. This system exhibits a continuous vapor−liquid critical line that connects the two pure component critical points in a nearly linear shape. At low temperatures, a locus of upper critical solution temperature (USCT) points is observed, indicating liquid−liquid immiscibility that runs from high pressures with an almost vertical slope to a UCEP ($T_{UCEP} = 212.2$ K and $P_{UCEP} = 3.88$

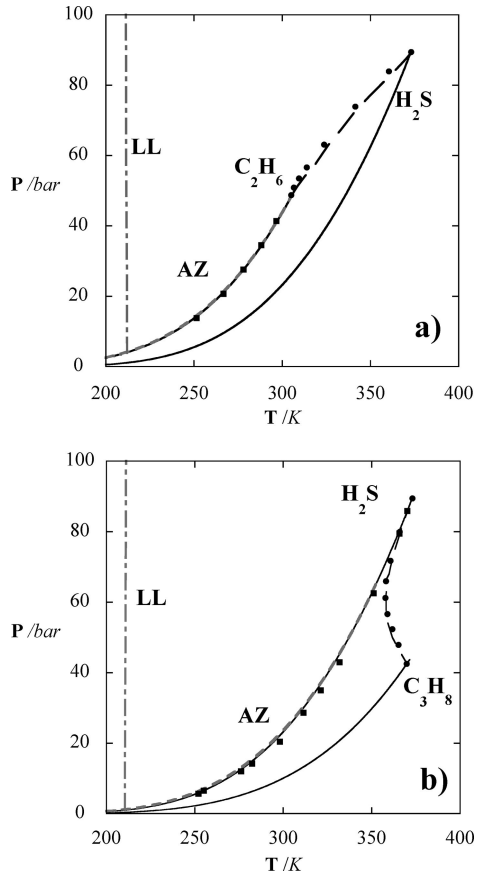

Figure 6. *PT* projection of the *PTx* surface of the binary mixtures of (a) H_2S (1) + ethane (2) and (b) H_2S (1) + propane (2). Circles and squares correspond to the experimental data[6,7,9–13] for the critical lines and azeotrope, respectively. Solid lines represent the SAFT-VR+D predictions for the vapor pressures of pure components; long-dashed lines, dashed lines, dotted line, and dashed-dotted lines correspond to the vapor−liquid critical lines, azeotrope lines, three-phase liquid−liquid−vapor line, and liquid−liquid critical line, respectively.

bar) on the three-phase (liquid−liquid−vapor) line. A locus of azeotropic points close to the vapor pressure curve of ethane is also observed. These features are characteristic of type II^A phase behavior in the Scott and Konynenburg classification. The azeotropic line runs from low to high temperatures where it merges with the critical gas−liquid line at a pressure of 49 bar and a temperature of 305.8 K, near the critical point of pure ethane (305.3 K and 48.8 bar[94]). As we can see from the figure, the liquid−liquid immiscilitity decreases as the molecular weight of the alkane increases, from complete immiscibility in the type *III* phase behavior observed for the H_2S + methane mixture, to partial immiscibility and type *II* behavior for the H_2S + ethane system. Although there is no experimental data for the liquid−liquid immiscibility predicted for this system, the vapor−liquid phase diagrams observed experimentally at pressures near the azeotropic locus are very flat which can be a sign of the presence of liquid−liquid immiscibility at low temperatures. Furthermore, in an experimental study of the H_2S + ethane system, Kaira et al.[7] found that it was very difficult to obtain reliable data at low temperatures (around 200 K) because of the fact that small changes in pressure lead to large changes in composition. Given the accuracy of the SAFT-VR+D predictions for the methane + H_2S phase diagram, we would anticipate accurate predictions for the ethane + H_2S binary mixture.

In part b of Figure 6, the *PT* projection of the *PTx* surface for the H_2S (1) + propane (2) binary mixture is shown. Similar to the ethane binary mixture, the theoretical results from the SAFT-VR+D approach predict a continuous vapor−liquid critical line that connects the two pure component critical points and an azeotrope line, with liquid−liquid immiscibility at low temperature (type II^A phase behavior). The critical locus passes through a minimum point in the temperature at 356.6 K, which is in excellent agreement with the experimental value of 357 K.[9] The azeotrope line is now located near the vapor pressure of pure hydrogen sulfide and runs from low to high temperatures until it merges to the vapor pressure curve of hydrogen sulfide, close to the gas−liquid critical locus. At low temperatures, liquid−liquid immiscibility runs from high pressures with an almost vertical slope to the UCEP (T_{UCEP} = 210.5 K and P_{UCEP} = 1.22 bar), where it terminates on the three-phase (liquid−liquid−vapor) line. Comparing the values of the UCEP for both systems, we see that the liquid−liquid immiscibility is reduced when ethane is replaced by propane. Again, given that we have only used Lorentz−Berthelot combining rules, the theory is in excellent agreement with the experimental data for the gas−liquid critical locus as well as the azeotrope line for these mixtures and accurately predicts the correct type of phase behavior.

The different azeotropic behavior observed for the hydrogen sulfide + ethane and hydrogen sulfide + propane systems is described more clearly in Figure 7, where a selected number of *Px* projections of the *PTx* surface for both mixtures are presented. Both mixtures show a pressure maximum, which is a feature of positive deviations from Raoult's law in mixtures of polar and nonpolar substances. The theoretical predictions of the *Px* slices of the phase diagram for both systems are in very good agreement with the experimental data. The shift in the azeotrope loci from the ethane rich, in the H_2S + ethane system, to the hydrogen sulfide rich phase, in the H_2S + propane system, is correctly predicted. Moreover, the quantitative agreement between the SAFT-VR+D predictions and the experimental data at these low temperatures is very good given that we are using rescaled parameters and that the theoretical calculations are pure predictions since we do not fit to any binary mixture data.

C. Hydrogen Sulfide + *n*-Butane up to *n*-Decane Binary Mixtures. We have also examined the phase equilibrium of hydrogen sulfide with longer *n*-alkanes. In Figure 8, we present the *PT* projection of the high-pressure critical lines from the H_2S + *n*-butane through to *n*-decane binary mixtures. As can be seen, the critical lines of the mixtures are continuous, going from the gas−liquid critical point of one pure component to the other. This behavior clearly indicates that all mixtures in this subsection exhibit type *I* phase behavior. Excellent agreement with experimental data is obtained for the prediction of the vapor−liquid critical lines for all of the mixtures except pentane. First, from these results, it is interesting to note the change of the curvature in the gas−liquid critical line for the hydrogen sulfide + *n*-butane mixture, which is related to the fact that the hydrogen sulfide + propane system exhibits a minimum temperature in the critical locus and azeotropic behavior. Second, it is also important to mention that the liquid−liquid immiscibility predicted in the hydrogen sulfide + propane system has shifted toward lower temperatures and pressures in the system hydrogen sulfide + *n*-butane, well below the triple point of hydrogen sulfide (187.66 K and 0.232 bar[94]) where the liquid−liquid immiscibility is pre-empted by the appearance of the solid phase. For the hydrogen sulfide + *n*-pentane binary mixture, the predicted critical locus exhibits a linear shape which differs from the experimental data,

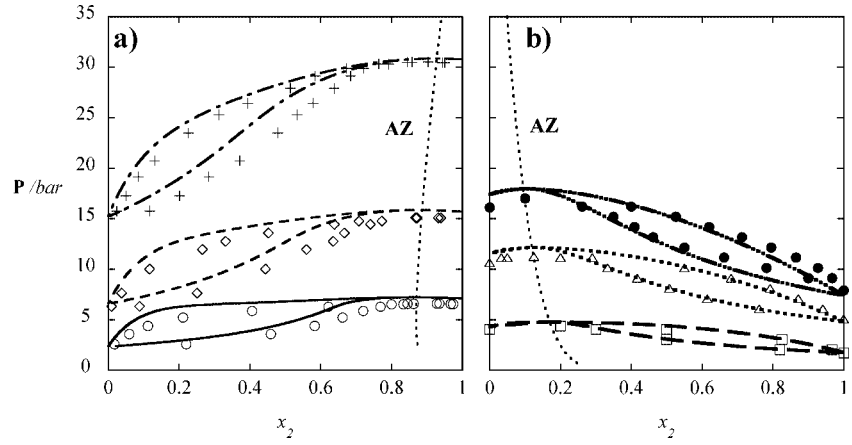

Figure 7. *Px* constant-temperature slices of the binary mixtures of (a) H_2S (1) + ethane (2) and (b) H_2S (1) + propane (2). Symbols represent the experimental data and lines correspond to the theoretical predictions from the SAFT-VR+D approach. The temperature values studied are 228.0 K (circles and solid lines), 244.0 K (squares and long dashed lines); 255.0 K (diamonds and dashed lines), 273.0 K (triangles and dotted lines), 283.0 K (crosses and dash-dotted lines), and 288.0 K (closed circles and dash-dot-dot-dot lines). The thin dotted lines represent theoretical predictions for the azeotrope locus.

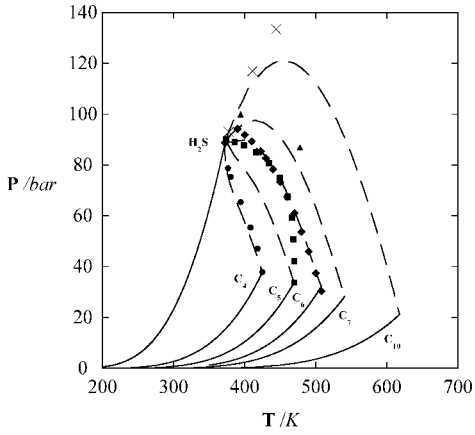

Figure 8. *PT* projection of the *PTx* surface for the binary mixtures of H_2S (1) + *n*-butane[14] (circles), + *n*-pentane[15] (squares), + *n*-hexane[16] (diamonds), + *n*-heptane[17–19] (triangles), and + *n*-decane[20] (crosses). Symbols correspond to the experimental data of the critical lines. Solid lines represent the SAFT-VR+D predictions for the vapor pressures of pure components; long dashed lines represent the vapor−liquid critical lines.

which shows an almost vertical line near the pure *n*-pentane critical point that then crosses the experimental data of the critical line for the hydrogen sulfide + *n*-hexane mixture. As can be seen from Figure 8, the theoretical predictions for the critical lines exhibit a more subtle change when the second component varies from *n*-butane up to *n*-hexane, which would be expected for mixtures within the same chemical family and therefore appears more natural than the crossing behavior observed in the experimental data, suggesting that the experimental data for the H_2S + pentane system could be in error. For the hydrogen sulfide + *n*-hexane up to *n*-decane binary mixtures, the gas−liquid critical lines show a maximum in pressure, and is related to the difference in interactions between the strongly polar hydrogen sulfide and the longer hydrocarbons which favor deviations from ideal behavior. This maximum moves toward higher temperatures and pressures as we increase the molecular weight of the *n*-alkane component. Again, it is important to note that the results for these systems are obtained using simple Lorentz−Berthelot combining rules to determine the phase behavior of mixtures from the pure components parameters and so clearly illustrate the ability of the SAFT-VR+D equation of state to accurately predict the phase behavior of these polar−nonpolar binary mixtures.

We have also studied a series of constant-temperature *Px* slices for H_2S + longer *n*-alkane binary mixtures. In Figure 9a, the theoretical predictions for hydrogen sulfide (1) + *n*-hexane (2) at constant temperatures of 323, 373, and 422 K are presented and are seen to be in good agreement with the experimental data. In part b, theoretical predictions for the hydrogen sulfide (1) + *n*-heptane (2) system at constant temperatures of 313, 333, 354, and 373 K are also shown. Again, the agreement between the theoretical predictions and the experimental data is good. For both systems, the theory is able to predict quantitatively the vapor-phase envelope but slightly underestimates the pressures for the liquid-phase behavior at high temperatures.

D. Solubility of Hydrogen Sulfide in Longer Linear Alkanes. Finally, we have also studied a number of constant-temperature *Px* slices of the *PTx* phase diagrams for mixtures of hydrogen sulfide with heavy *n*-alkanes. Figure 10 shows the gas−liquid phase behavior of hydrogen sulfide and (a) *n*-decane, (b) *n*-tridecane, (c) *n*-hexadecane, and (d) *n*-eicosane. These figures correspond to the solubility of hydrogen sulfide in each *n*-alkane over a wide range of temperatures. The agreement between the results from the SAFT-VR+D approach and the experimental data is good considering that we have not adjusted any of the model parameters to experimental mixture data and that we are using parameters rescaled to the pure component critical points. Although, there is an underestimation of the pressure for the liquid-phase behavior that can be overcome by using the optimized (i.e., not rescaled) intermolecular parameters, which will improve the predictions for the liquid phase densities of pure hydrogen sulfide (Figure 3b). Nonetheless, the theory is able to qualitatively predict the experimentally observed behavior as a function of temperature: the solubility of hydrogen sulfide increases as the temperature decreases. In the work of Nath et al.,[72] molecular simulations of the hydrogen sulfide + *n*-dodecane system exhibited a similar trend with temperature: the solubility increases with a decrease in temperature. This increase in the solubility of hydrogen sulfide could be due to increased association interactions between hydrogen sulfide molecules at low temperature that force the H_2S molecules to prefer the liquid

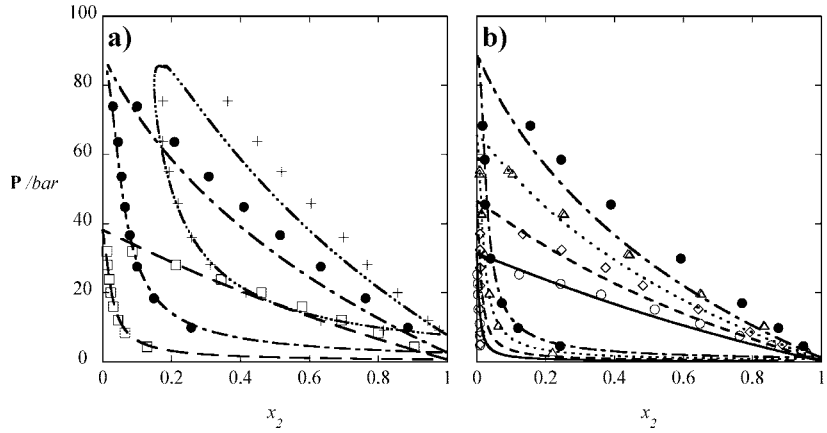

Figure 9. *Px* constant-temperature slices of the binary mixtures of (a) H_2S (1) + *n*-hexane (2) and (b) H_2S (1) + *n*-heptane (2). Symbols represent the experimental data[16–19] and lines correspond to the theoretical predictions using the SAFT-VR+D approach. The temperature values studied are 313.0 K (circles and solid lines), 323.0 K (squares and long dashed lines), 333.0 K (diamonds and dashed lines), 354.0 K (triangles and dotted lines), 373.0 K (closed circles and dash-dotted lines), and 422.0 K (crosses and dash-dot-dot-dot lines).

phase. Additionally, a comparison between Figure 10a−c at a fixed temperature (323, 373, or 423 K) shows how the solubility increases as the molecular weight of the second component of the mixture (*n*-alkane) increases as we change from *n*-decane to *n*-hexadecane.

IV. Conclusions

In this work, we have extended the SAFT-VR+D approach to describe with mixtures of polar and nonpolar fluids. In particular, we have examined the thermodynamic properties of the hydrogen sulfide + *n*-alkane binary mixtures and find that the SAFT-VR+D approach is able to accurately predict the phase behavior of the systems studied. The molecular parameters for hydrogen sulfide were determined by fitting to experimental vapor pressure and saturated liquid density data, using the experimental value for the dipole moment, while the parameters for the *n*-alkanes were taken from previous work.[64,65] Since our main interest is in the critical lines, we have used parameters rescaled to the experimental critical points of the pure components with standard Lorentz−Berthelot combining rules to obtain the unlike interaction parameters from the pure component parameters.

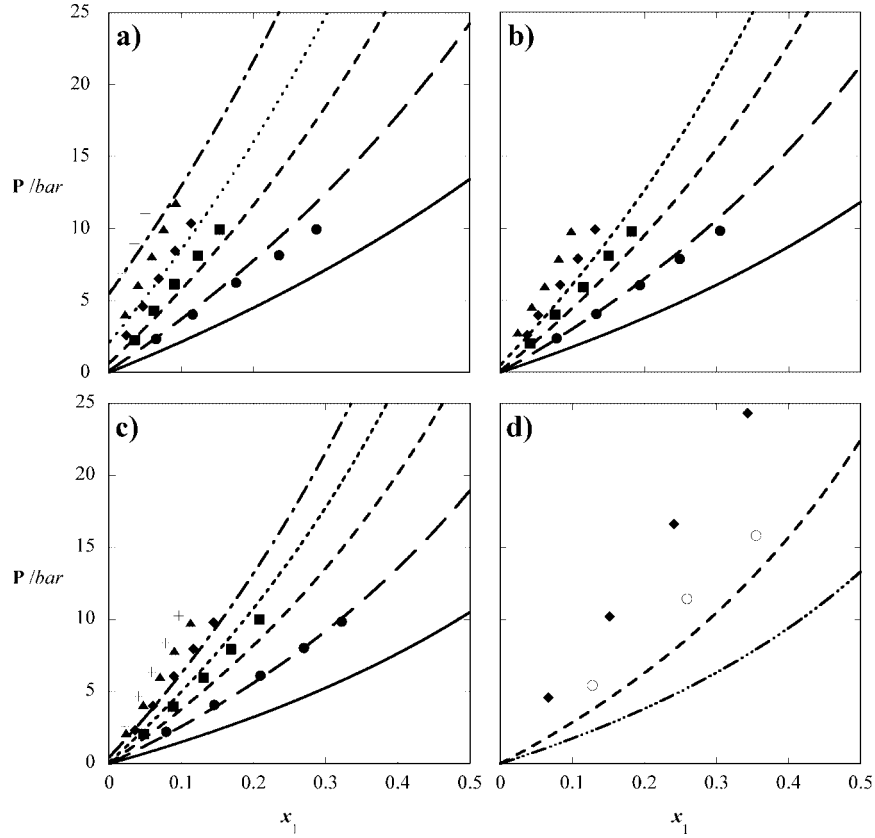

Figure 10. Solubility of hydrogen sulfide in (a) *n*-decane, (b) *n*-tridecane, (c) *n*-hexadecane, and (d) *n*-eicosane. Symbols represent the experimental data[20,21] and lines correspond to the theoretical predictions using the SAFT-VR+D approach. The temperature values studied are 323.15 K (circles and solid lines), 361.15 K (open circles and dash-dotted lines), 373.15 K (squares and long dashed lines), 423.15 K (diamonds and dashed lines), 473.15 K (triangles and dotted lines), 573.15 K (crosses and dash-dot-dot-dot lines).

The theoretical results show that the global phase diagrams of the hydrogen sulfide + *n*-alkane systems exhibit a rich phase behavior: type *III* phase behavior, according to the classification of Scott and van Konynenburg, for H_2S + methane; type *II* with azeotropy for H_2S + ethane and H_2S + propane systems; and finally type *I* for H_2S + *n*-butane up to *n*-decane. The SAFT-VR+D theory accurately predicts the experimentally observed type *III* phase behavior for the H_2S + methane phase diagram and the type *I* behavior observed for the H_2S + *n*-butane, *n*-pentane, *n*-hexane, *n*-heptane, and *n*-decane. We also find that the SAFT-VR+D approach predicts a smoother transition between the vapor−liquid critical lines of the H_2S + *n*-butane, + *n*-pentane, and + *n*-hexane systems than those observed experimentally, suggesting that reliability of the experimental data for the H_2S + *n*-pentane system should be questioned. Although experimental data exists for the H_2S + ethane and H_2S + propane systems, the SAFT-VR+D prediction of liquid−liquid immiscibility, and therefore type *II* phase behavior, has not been verified experimentally; the theoretical predictions provide a reliable prediction for the phase behavior of these systems for which experimental measurements are difficult.

Finally, we have also studied the solubility of H_2S in heavier *n*-alkanes, from *n*-decane up to *n*-eicosane. The SAFT-VR+D theory was able to explore and predict, in a qualitative manner, the effect of temperature and the molecular weight of the hydrocarbon component on the solubility of H_2S in the *n*-alkanes. In future work, we will further test the accuracy of the SAFT-VR+D approach through the study of mixtures involving both polar chain fluids, such as alcohols, and systems in which both components are polar.

Acknowledgment. We gratefully acknowledge financial support from the National Science Foundation under Grant CTS-0452688 and an REU supplement to CTS-0453641. We also thank Nurhikmah Mohd Hanifiah for her help in the preliminary stages of this work.

References and Notes

(1) Jones, D. S. J.; Pujadú, P. P. *Handbook of petroleum processing*, 1st ed.; Springer: New York, 2006.
(2) Al-Awadhy, F.; Kocabas, I.; Abou-Kassem, J. H.; Islam, M. R. *Energy Sources* **2005**, *27*, 3.
(3) Kent, J. A. *Riegel's handbook of industrial chemistry*, 10th ed.; Springer: New York, 2003.
(4) Kohn, J. P.; Kurata, F. *AIChE J.* **1958**, *4*, 211.
(5) Reamer, H. H.; Sage, B. H.; Lacey, W. N. *Ind. and Eng. Chem.* **1951**, *43*, 976.
(6) Kay, W. B.; Brice, D. B. *Ind. and Eng. Chem.* **1953**, *45*, 615.
(7) Kaira, H.; Robinson, D. B.; Krishnan, T. R. J. *Chem. Eng. Data* **1977**, *22*, 85.
(8) Rivollet, F.; Jarne, C.; Richon, D. J. *Chem. Eng. Data* **2005**, *50*, 1883.
(9) Kay, W. B.; Rambosek, G. M. *Ind. and Eng. Chem.* **1953**, *45*, 221.
(10) Carroll, J. J.; Mather, A. E. *Fluid Phase Equilib.* **1992**, *81*, 187.
(11) Brewer, J.; Rodewald, N.; Kurata, F. *AIChE J.* **1961**, *7*, 13.
(12) Jou, F.-Y.; Carroll, J. J.; Mather, A. E. *Fluid Phase Equilib.* **1995**, *109*, 235.
(13) Gilliland, E. R.; Scheeline, H. W. *Ind. and Eng. Chem.* **1940**, *32*, 48.
(14) Leu, A.-D.; Robinson, D. B. J. *Chem. Eng. Data* **1989**, *34*, 315.
(15) Reamer, H. H.; Sage, B. H.; Lacey, W. N. *Ind. and Eng. Chem.* **1953**, *45*, 1805.
(16) Laugier, S.; Richon, D. J. *Chem. Eng. Data* **1995**, *40*, 153.
(17) Kaira, H.; Kubota, H.; Robinson, D. B.; Ng, H.-J. J. *Chem. Eng. Data* **1978**, *23*, 317.
(18) Ng, H.-J.; Kalra, H.; Robinson, D. B.; Kubota, H. J. *Chem. Eng. Data* **1980**, *25*, 51.
(19) Theveneau, P.; Coquelet, C.; Richon, D. *Fluid Phase Equilib.* **2006**, *249*, 179.
(20) Yokoyama, C.; Usui, A.; Takahashi, S. *Fluid Phase Equilib.* **1993**, *85*, 257.
(21) Feng, G.-x.; Mather, A. E. *J. Chem. Eng. Data* **1992**, *37*, 412.
(22) Feng, G.-X.; Mather, A. E. *Fluid Phase Equilib.* **1993**, *87*, 341.
(23) Lee, J. I.; Mather, A. E. *Ber. Bunsen-Ges. Phys. Chem.* **1977**, *81*, 1020.
(24) Bierlein, J. A.; Kay, W. B. *Ind. and Eng. Chem.* **1953**, *45*, 618.
(25) Scott, R. L.; van Konynenburg, P. H. *Discuss. Faraday Soc.* **1970**, *49*, 87.
(26) van Konynenburg, P. H.; Scott, R. L. *Phil. Trans.* **1980**, *A298*, 495.
(27) Rowlinson, J. S.; Swinton, F. L. *Liquids and liquid mixtures;* Butterworth Scientific: London, 1982; Vol. 3rd ed.
(28) Jackson, G.; Chapman, W. G.; Gubbins, K. E. *Mol. Phys.* **1988**, *65*, 1.
(29) Chapman, W. G.; Gubbins, K. E.; Jackson, G.; Radosz, M. *Ind. Eng. Chem. Res.* **1990**, *29*, 1709.
(30) Wertheim, M. S. *J. Stat. Phys.* **1984**, *35*, 19.
(31) Wertheim, M. S. *J. Stat. Phys.* **1984**, *35*, 35.
(32) Wertheim, M. S. *J. Stat. Phys.* **1986**, *42*, 459.
(33) Wertheim, M. S. *J. Stat. Phys.* **1986**, *42*, 477.
(34) Sengers, J. V.; Kayser, R. F.; Peters, C. J.; White, H. J. *Equations of state for fluids and fluid mixtures*; Elsevier: Amsterdam, 2000.
(35) Müller, E. A.; Gubbins, K. E. *Ind. Eng. Chem. Res.* **2001**, *40*, 2193.
(36) Economou, I. G. *Ind. Eng. Chem. Res.* **2002**, *41*, 953.
(37) Clark, G. N. I.; Haslam, A. J.; Galindo, A.; Jackson, G. *Mol. Phys.* **2006**, *104*, 3561.
(38) García-Lisbona, M. N.i.; Galindo, A.; Jackson, G.; Burges, A. N. *Mol. Phys.* **1998**, *93*, 57.
(39) McCabe, C.; Galindo, A.; Cummings, P. T. *J. Phys. Chem. B* **2003**, *107*, 12307.
(40) McCabe, C.; Kiselev, S. B. *Ind. Eng. Chem. Res.* **2004**, *43*, 2839.
(41) Galindo, A.; Gil-Villegas, A.; Whitehead, P. J.; Jackson, G.; Burgess, A. N. *J. Phys. Chem. B* **1998**, *102*, 7632.
(42) Galindo, A.; Blas, F. J. *J. Phys. Chem. B* **2002**, *106*, 4503.
(43) Blas, F. J.; Galindo, A. *Fluid Phase Equilib.* **2002**, *194−197*, 501.
(44) Sun, L. X.; Zhao, H. G.; Kiselev, S. B.; McCabe, C. *J. Phys. Chem. B* **2005**, *109*, 9047.
(45) dos Ramos, M. C.; Blas, F. J.; Galindo, A. *J. Phys. Chem. C* **2007**, *111*, 15924.
(46) dos Ramos, M. C.; Blas, F. J.; Galindo, A. *Fluid Phase Equilib.* **2007**, *261*, 359.
(47) Kraska, T.; Gubbins, K. E. *Ind. Eng. Chem. Res.* **1996**, *35*, 4738.
(48) Kraska, T.; Gubbins, K. E. *Ind. Eng. Chem. Res.* **1996**, *35*, 4727.
(49) Müller, E. A.; Gubbins, K. E. *Ind. Eng. Chem. Res.* **1995**, *34*, 3662.
(50) Xu, K.; Li, Y.-G.; Liu, W.-B. *Fluid Phase Equilib.* **1998**, *142*, 55.
(51) Gross, J.; Vrabec, J. *AIChE Journal* **2006**, *52*, 1194.
(52) Karakatsani, E. K.; Spyriouni, T.; Economou, I. G. *AIChE J.* **2005**, *51*, 2328.
(53) Karakatsani, E. K.; Economou, I. G. *J. Phys. Chem. B* **2006**, *110*, 9252.
(54) Gubbins, K. E.; Gray, C. G. *Mol. Phys.* **1972**, *23*, 187.
(55) Stell, G.; Rasaiah, J. C.; Narang, H. *Mol. Phys.* **1972**, *23*, 393.
(56) Jog, P. K.; Chapman, W. G. *Mol. Phys.* **1999**, *97*, 307.
(57) Jog, P. K.; Sauer, S. G.; Blaesing, J.; Chapman, W. G. *Ind. Eng. Chem. Res.* **2001**, *40*, 4641.
(58) Tumakaka, F.; Sadowski, G. *Fluid Phase Equilib.* **2004**, *217*, 233.
(59) Zhao, H.; McCabe, C. *J. Chem. Phys.* **2006**, *125*, 4504.
(60) Zhao, H. G.; Ding, Y.; McCabe, C. *J. Chem. Phys.* **2007**, *127*, 4514.
(61) Zhao, H. G.; dos Ramos, M. C.; McCabe, C. *J. Chem. Phys.* **2007**, *126*, 4503.
(62) Adelman, S. A.; Deutch, J. M. *J. Chem. Phys.* **1973**, *59*, 3971.
(63) Benavides, A. L.; Guevara, Y. *J. Phys. Chem. B* **2003**, *107*, 9477.
(64) Gil Villegas, A.; Galindo, A.; Whitehead, P. J.; Mills, S. J.; Jackson, G.; Burgess, A. N. *J. Chem. Phys.* **1997**, *106*, 4168.
(65) McCabe, C.; Jackson, G. *Phys. Chem. Chem. Phys.* **1999**, *1*, 2057.
(66) Jorgensen, W. L. J. *Phys. Chem.* **1986**, *90*, 6379.
(67) Forester, T. R.; McDonald, I. R.; Klein, M. L. *129* **1989**, 225.
(68) Kristof, T.; Liszi, J. J. *Phys. Chem. B* **1997**, *101*, 5480.
(69) Jorgensen, W. L.; Chandrasekhar, J.; Madura, J. D.; Impey, R. W.; Klein, M. L. *J. Chem. Phys.* **1983**, *79*, 926.
(70) Kamath, G.; Potoff, J. J. *Fluid Phase Equilib.* **2006**, *246*, 71.
(71) Delhommelle, J.; Boutin, A.; Fuchs, A. H. *Mol. Simul.* **1999**, *22*, 351.
(72) Nath, S. K. *J. Phys. Chem. B* **2003**, *107*, 9498.
(73) Ungerer, P.; Nieto-Draghi, C.; Lachet, V.; Wender, A.; Lella, A. D.; Boutin, A.; Rousseau, B.; Fuchs, A. H. *Mol. Simul.* **2007**, *33*, 287.
(74) Ungerer, P.; Nieto-Draghi, C.; Rousseau, B.; Ahunbay, G.; Lachet, V. J. *Mol. Liq.* **2007**, *134*, 71.
(75) Aparicio-Martinez, S.; Hall, K. R. *Ind. Eng. Chem. Res.* **2007**, *46*, 291.
(76) Huang, S. H.; Radosz, M. *Ind. Eng. Chem. Res.* **1990**, *29*, 2284.
(77) Tihic, A.; Kontogeorgis, G. M.; von Solms, N.; Michelsen, M. L. *Fluid Phase Equilib.* **2006**, *248*, 29.

(78) Archer, A. L.; Amos, M. D.; Jackson, G.; McLure, I. A. *Int. J. Thermophys.* **1996**, *17*, 201.
(79) Jackson, G.; Gubbins, K. E. *Pure Appl. Chem.* **1989**, *61*, 1021.
(80) Gray, C. G.; Gubbins, K. E. *Theory of molecular fluids: Fundamentals volume i*; Oxford University Press: New York, 1985.
(81) Galindo, A.; Davies, L. A.; Gil-Villegas, A.; Jackson, G. *Mol. Phys.* **1998**, *93*, 241.
(82) Hansen, J. P.; McDonald, I. R. Theory of simple liquids; Academic Press: London, 1990; Vol. 2nd ed.
(83) Barker, J. A.; Henderson, D. *J. Chem. Phys.* **1967**, *47*, 2856.
(84) Barker, J. A.; Henderson, D. *J. Chem. Phys.* **1967**, *47*, 4714.
(85) Barker, J. A.; Henderson, D. *Rev. Mod. Phys.* **1976**, *48*, 587.
(86) Boublik, T. *J. Chem. Phys.* **1970**, *53*, 471.
(87) Mansoori, G. A.; Carnahan, N. F.; Starling, K. E.; Leland, T. W. *J. Chem. Phys.* **1971**, *54*, 1523.
(88) Wertheim, M. S. *J. Chem. Phys.* **1971**, *55*, 4291.
(89) Gulley, R. J.; Brunger, M. J.; Buckman, S. J. *J. Phys. B* **1993**, *26*, 2913.
(90) Kirkpatrick, S.; Gelatt, C. D.; Vecchi, M. P. *Science* **1983**, *220*, 671.
(91) Dolan, W. B.; Cummings, P. T.; Levan, M. D. *AIChE Journal* **1989**, *35*, 725.
(92) McCabe, C.; Kiselev, S. B. *Fluid Phase Equilib.* **2004**, *219*, 3.
(93) Sun, L. X.; Zhao, H. G.; Kiselev, S. B.; McCabe, C. *Fluid Phase Equilib.* **2005**, *228*, 275.
(94) http://webbook.nist.gov/chemistry/. Nist chemistry webbook, 1991.
(95) McCabe, C.; Galindo, A.; Gil-Villegas, A.; Jackson, G. *J. Phys. Chem. B* **1998**, *102*, 8060.
(96) McCabe, C.; Gil-Villegas, A.; Jackson, G. *J. Phys. Chem. B* **1998**, *102*, 4183.
(97) McCabe, C.; Galindo, A.; Gil-Villegas, A.; Jackson, G. *Int. J. Thermophys.* **1998**, *19*, 1511.
(98) Sage, B. H.; Lacey, W. N. *Some properties of the lighter hydrocarbons, hydrogen sulfide, and carbon dioxide*; American Petroleum Institute: New York, 1955.
(99) Beaton, C. F.; Hewitt, G. F. *Physical property data for the design engineer*; Hemisphere Publishing Corp.: New York, 1989.

JP800397N